Phobos and Deimos surface composition: search for spectroscopic analogues

Giovanni Poggiali, M Matsuoka, M A Barucci, J R Brucato, P Beck, S Fornasier, A Doressoundiram, F Merlin, A Alberini

Monthly Notices of the ROYAL ASTRONOMICAL SOCIETY

MNRAS **516,** 465–476 (2022) https://doi.org/10.1093/mnras/stac2226
Advance Access publication 2022 August 10

Phobos and Deimos surface composition: search for spectroscopic analogues

Giovanni Poggiali [1]★ M. Matsuoka,[1,2] M. A. Barucci [1] J. R. Brucato,[3] P. Beck,[4] S. Fornasier [1,5] A. Doressoundiram [1] F. Merlin[1] and A. Alberini[3,6]

[1]*LESIA-Observatoire de Paris, Université PSL, CNRS, Université Paris Cité, Sorbonne Université, 5 place Jules Janssen, F-92190 Meudon, France*
[2]*The Geological Survey of Japan, National Institute of Advanced Industrial Science and Technology, 1-1-1 Higashi, Tsukuba 305-8567, Japan*
[3]*INAF-Astrophysical Observatory of Arcetri, largo E. Fermi n.5, I-50125 Firenze, Italy*
[4]*Institut de Planétologie et d'Astrophysique de Grenoble, OSUG/CNRS, 122 rue de la piscine, F-38000 Grenoble, France*
[5]*Institut Universitaire de France (IUF), 1 rue Descartes, F-75231 Paris Cedex 05, France*
[6]*Dipartimento di Fisica ed Astronomia, Università degli Studi di Firenze, Via Sansone n.1, I-50019 Sesto Fiorentino (Firenze), Italy*

Accepted 2022 July 18. in original form 2022 June 14

ABSTRACT

Phobos and Deimos, the two satellites of Mars, were largely studied in the past using ground-based telescope and spacecraft data, although most of the data were obtained by opportunity observations performed by Mars dedicated orbiters. Despite the data available so far, the main composition of the two moons is not yet fully understood. The possible presence of hydrated minerals along with mafic minerals olivine and pyroxene seems to be the most plausible interpretation, but more investigations are needed. MIRS spectrometer on-board the future JAXA MMX sample return mission will help to unveil the open question on the composition of Phobos and Deimos. In this work, we review past spectroscopic observations of the Martian moons, both from ground observatories and spacecraft data set, aiming at better understanding the constraints in interpreting the Mars satellites composition and at identifying the best spectroscopic analogues. We also present new laboratory measurements on mineral mixing and meteorites to match the satellites spectral behaviour. New measurements were acquired at INAF-Astrophysical Observatory of Arcetri and IPAG laboratories at room conditions exploring different geometries and the results obtained set new constraints for future laboratory measurements. Our preliminary results confirm that the surface of Phobos and Deimos can be associated with samples characterized by a higher presence of dark components (e.g. amorphous carbon) or minerals produced by space weathering (e.g. Fe0 and FeS-bearing materials). Presence of dark component could also be totally responsible for the reduced hydrated band observed on the moons without invoking dehydration or OH-implantation on anhydrous surface.

Key words: methods: laboratory: solid state – space vehicles: instruments – techniques: imaging spectroscopy – planets and satellites: composition – planets and satellites: individual: Phobos – planets and satellites: surfaces.

1 INTRODUCTION

Nowadays, there is still an open debate on the origin of Phobos and Deimos, the two moons of Mars. Unlike Earth's Moon, they are small irregularly shaped objects with a mean radius of about 11 km for Phobos and 6 km for Deimos (about 56 per cent of the size of Phobos). Phobos is heavily cratered with the biggest crater, named Stickney, reaching 9 km in diameter. On the other hand, Deimos is cratered too, but the surface is noticeably smoother than that of Phobos. Several theories were proposed but without a general agreement on the moons' origin and evolution. The two main hypotheses about Phobos and Deimos genesis involve a giant impact between Mars and a planetesimal (Rosenblatt et al. 2016; Hesselbrock & Minton 2017; Hyodo et al. 2018; and reference therein) and the possible capture of primitive asteroids (Hartmann 1990; Higuchi & Ida 2017). Both theories have pros and cons: the orbits of Phobos and Deimos are well explained by the giant impact theory but it fails to properly justify composition and spectral properties of the two moons. The captured asteroid hypothesis accounts easily for the spectral properties, but is not that simple to demonstrate from a dynamical point of view at the present orbital state of the Mars system.

JAXA MMX mission (Kuramoto et al. 2022) will clarify the origins of Martian moons and better understand the Martian system. Indeed, along with a suite of scientific instruments on-board the spacecraft, MMX will perform two sample collections from Phobos, the largest moon, returning the samples back to Earth in 2029. Waiting for MMX arrival, one of the most challenging open topics is to constrain the composition of the two moons, which is directly linked with the debate about their origin. To address it, several observations were performed in the past both in the near-infrared and thermal infrared range, using ground-based telescopes and instruments on-board spacecrafts orbiting the Martian system. We will review in the next section the most relevant observations of Phobos and Deimos and the derived results. Then we will present some new laboratory measurements performed as preliminary work in order to investigate possible spectroscopic analogues for Phobos

★ E-mail: giovanni.poggiali@obspm.fr

and Deimos. This work will also support the scientific investigation of MIRS spectrometer (Barucci et al. 2021) on-board MMX spacecraft.

1.1 Spectroscopic observations of Phobos and Deimos

Early observations of Martian moons were made by several space missions arriving in proximity of the Red Planet from the 1960s, but Phobos-2, the first mission completely dedicated to exploring the Martian moons, arrived in the system only in 1989. The spacecraft was carrying an ultraviolet-visible point spectrometer (KRFM) covering the 0.33–0.60 μm wavelength range, and a near-infrared imaging spectrometer (ISM) covering the 0.76–3.16 μm wavelength range. These two instruments provided the first series of resolved spectroscopic observations of Phobos surfaces. Authors working on data collected by these instruments were describing a featureless spectrum with a red slope but failed in finding a good analog among meteorites collections, and suggested a possible iron-bearing silicate composition mixed with carbon and/or its compounds (Bibring et al. 1992). Moreover, two distinct spectral units were observed: A 'redder unit' with a visible/near-infrared colour ratio of 0.6−0.85 and a 'bluer' unit with a visible/near-infrared colour ratio of 0.85−1.2. The former was associated with the most superficial layer and the latter, being associated with the large Stickney impact crater, was linked with fresher material that originated in the deeper layer of Phobos (Murchie et al. 1991). Phobos' red unit was associated with T-type asteroids, a class of dark bodies with low-albedo and a moderate red slope in Tholen (1984) taxonomy. The main hypothesis was a mafic-rich composition with high degree of space weathering or a mixture of mafic-poor and mafic-rich material (Murchie & Erard 1996).

Joining Phobos2 data with measurements from Imager for Mars Pathfinder, ground observations and *Hubble Space Telescope* observations, a correlation between Phobos and C-type asteroids was excluded due to the differences in spectral slope (Murchie 1999; Thomas et al. 1999). The presence of a possible absorption feature near 0.7 μm was also suggested. A spectroscopic comparison was made with both the D-type asteroids, which also have a steep spectral slope and are supposed to be primordial and organic-rich bodies, and highly space weathered mafic-rich assemblages, the latter corroborated by a weak absorption feature at about 1 μm linked with olivine and/or pyroxene (Murchie 1999). Deimos spectrum was found to be close to Phobos red unit and therefore to D-type asteroids confirming previous observations (Pang et al. 1980; Lucey, Bell & Piscitelli 1989; Grundy & Fink 1992). More recent reinvestigation of ISM data identified in localized regions of Phobos surface two absorption bands at 1.04 and 1.9 μm interpreted as a mixture of low-calcium pyroxene and olivine. A variation in the relative proportions of the two components was found and the concentration of olivine seems to be globally higher than the concentration of pyroxene in the low-albedo regions (Gendrin, Langevin & Erard 2005). A possible hydrated band was tentatively identified in several areas. However, this observation was defined by the authors as a 'possible clue' rather than an objective result (Gendrin et al. 2005).

Since the 2000s new ground observational campaigns have been performed on both moons. Rivkin et al. (2002) found no $-$ μm absorption feature due to hydrated minerals (with a limit on band depth of roughly $\sim$ 5–10 per cent on Phobos and $\sim$ 10–20 per cent on Deimos). Authors suggested that the leading side of Phobos, dominated by the Stickney crater, could be best matched by T-class asteroids, while spectral slopes of the trailing side of Phobos and leading side of Deimos are closer to the spectra of D-class asteroids albeit with many open questions (Rivkin et al. 2002). These findings were partially confirmed by recent observations published by Takir et al. (2022), who confirm the strong similarity between Deimos spectrum and the Phobos red unit one, suggesting a similarity to D-type asteroids. They however detect a 3-μm band with a depth of 4–5 per cent on Deimos spectrum can be attributed to hydrated minerals in the bulk composition, to OH implanted from solar wind (Nakauchi et al. 2021) or even to delivery of hydrated exogenic material (McCord et al. 2012). Surprisingly no indication of mafic composition arises from their observations (Takir et al. 2022). Authors also report surface heterogeneities on Phobos, with a significant slope variation at shorter wavelengths possibly linked with different regolith's composition, and/or space weathering degree (Takir et al. 2022). Observations in the range of 1–13 μm for Deimos and 3–13 μm for Phobos revealed higher than expected temperatures but consistent with previous observations while, within the errors, there was little evidence for spectral features indicative of surface composition (Lynch et al. 2007).

As can be guessed from the observations just summarized, many doubts and inconsistencies arise from ground-based observations, and data from the first orbiters' observations were not sufficient to identify an unambiguous composition for the two moons. The arrival in the Mars system of two spacecrafts: Mars Express (MEX) and Mars Reconnaissance Orbiter, respectively, carrying the Observatoire pour la Mineralogie, l'Eau, les Glaces et l'Activité (OMEGA; Bibring et al. 2004), and the Compact Reconnaissance Imaging Spectrometer (CRISM, Murchie et al. 2007), provided in the last 20 yr a new data set of the Martian moons (Witasse et al. 2014; Murchie et al. 2008; Thomas et al. 2011). A first joint analysis of data from both instruments found low single scattering albedos and red slopes consistent with previous studies, as well as a lack of mafic mineral absorptions or OH or H_2O features. These results and the match with laboratory spectra of Tagish Lake that is usually suggested as an analog of D-type asteroids, point out towards a primitive composition for Phobos and Deimos (Fraeman et al. 2012). Subsequent analysis revealed the presence of weak absorption features in the range of 0.4–3.9 μm. Although no olivine and pyroxene Fe_2^+ electronic absorption were detected, other features were identified: a 0.65 μm broad-band, and a 2.8 μm metal-OH band, diagnostic of hydrated minerals, less intense in Phobos blue unit (Fraeman et al. 2014). The band at 0.65 μm was confirmed in the same work with dedicated ground observations (Fraeman et al. 2014). Two possible hypotheses were suggested to explain those observed features: highly desiccated Fe-phyllosilicate minerals or strong exogenic space weathering process that may induce the production of *Fe* and *OH* on the surface (Fraeman et al. 2014). In some preliminary works combining OMEGA data with UV data from SPICAM instrument on-board MEX a possible broad absorption band centred at 0.350 μm hints of a resemblance with some type of ilmenites although the feature fall in the data gap between 0.312 μm (end of SPICAM) and 0.390 μm (short end of OMEGA) and it was not subject of deeper analysis (Bertaux et al. 2016). A maximum in reflectance at 0.280 μm for Phobos and 0.260 μm for Deimos was also observed while a possible band at 0.220 μm is still under discussion (Bertaux et al. 2016). Recently, Pajola et al. (2018), using spectral modelling of CRISM data (between 0.5 and 2.5 μm), obtained a best fit with relative percentage of pyroxene glass (*PM*80) from 12 per cent to 18 per cent and Tagish Lake meteorite from 88 per cent to 82 per cent. Moreover, there is only a slight difference between the reddest and bluest slopes and it can be more characterized by a difference in grain size rather than a distinct dichotomy between the areas. Also a possible band between 1.6 and 1.9 μm (but still within the $\pm 1\sigma$ values) suggests a possible third

component (Pajola et al. 2018). The spectral modelling confirms results obtained from analysis of previously presented data merged with opportunity observations made with OSIRIS-NAC camera on-board *Rosetta* spacecraft (Pajola et al. 2013). Phobos' red slope, although redder than the average D-type asteroid, is found within the spectral dispersion of the D-types group (Pajola et al. 2012, 2013).

In parallel to near-infrared observations of the Martian moons some thermal infrared observations were performed. Lunine, Neugebauer & Jakosky (1982) using Viking Orbiter Infrared Thermal Mapper retrieved thermal inertia for both the moons. Phobos values were measured in the range between 40 and 70 $J\,K^{-1}\,m^{-2}\,s^{1/2}$, while Deimos values were in the range between 25 and 84 $J\,K^{-1}\,m^{-2}\,s^{1/2}$. This suggest that both moons are covered by a uniform layer of several cm of finely divided material (50–100 μm particle size). These results were confirmed by data from Phobos-2 spacecraft (Ksanfomality et al. 1989, 1991). Differences between brightness temperature at different wavelengths on Phobos were supposed to be induced by areas with high inertia or blocky material (Lunine et al. 1982). Contrary to results in near-infrared range, Phobos spectra acquired at longer wavelength show a large number of features, consistent with the abundant presence of fine grain dust (< 100 μm) on the surface of Phobos, and presumably Deimos. Early results of the Thermal Emission Spectrometer (TES) instrument (Christensen et al. 1992) on-board Mars Global Surveyor suggest that Phobos thermal emission spectrum is more consistent with silicates than organic refractory materials (Roush & Hogan 2000) with some variability observed in the region of Stickney crater (Roush & Hogan 2001). Combining TES observations with data from Planetary Fourier Spectrometer (PFS; Formisano et al. 2005), a more detailed analysis was possible. Both instruments have a good agreement when observing the same region and spectra are consistent with the presence of phyllosilicates (Giuranna et al. 2011). Although the presence of tectosilicates, especially feldspars, was confirmed by fitting the spectra obtained by several orbits and in addition the position of the Christiansen Feature (CF) in the TES data suggests ultramafic rock types (Giuranna et al. 2011). Re-analysis of TES data and laboratory comparison suggested the possibility of a general finely particulate basalt component mixed with a phyllosilicate component on the surface of Phobos. Moreover, the presence in the spectrum of several small peaks between 6 and 8 μm may indicate the presence of minor carbonate and hydrated alteration phases possibly more intense in red unit spectra (Glotch et al. 2018). Based on TES observations the thermal inertia of Phobos trailing hemisphere was mapped and the average value estimated around 70 $J\,K^{-1}\,m^{-2}\,s^{1/2}$ (Smith et al. 2018).

Summarizing more than 40 yr of observations of both the Martian moons, it appears evident that many open questions arise on their possible composition, as that some observations produce results not always in agreement.

1.2 Martian moons laboratory analogues

Although the possibility of material from Phobos and Deimos on Earth cannot be excluded (Wiegert & Galiazzo 2017), up to now no reliable meteorite analog of the Martian moons was found and only some hypotheses were proposed but with no spectroscopic match (Ivanov 2004). Observing a composite spectrum of Phobos, we notice immediately a predominance of spectral features in the thermal infrared and almost a total absence of bands in the visible and near-infrared. This dichotomy can be explained considering that some of the strongest bands in near-infrared are linked either with electronic transitions of Fe-bearing minerals (like pyroxene) and with the presence of hydrated minerals and/or organics/carbonates: if the surfaces of Phobos and Deimos are dessicated, poor in organics and carbonates and/or poor in Fe, then the spectrum in the region between 1 and 5 μm will appear featureless or with a reduced spectral contrast. Moreover, the presence of an opaque component on the surface (metals, iron oxides, amorphous carbon, etc.), derived from bulk composition or as a product of space weathering, can effectively reduce the band contrast in this wavelength region (e.g. Cloutis et al. 1990a, 2009). Additionally, if the minerals on the surface are fine grained, as expected by measured thermal properties (Lunine et al. 1982), or if they lose their crystalline structure (i.e. amorphized or glassed material) as the possible consequence of intense meteoritic bombardment, the spectral contrast will be severely reduced (e.g. Cloutis et al. 1990b). One or several of these conditions can lead to the observed featureless spectra of the two moons. However, in recent years some studies were performed to identify possible spectral analogs of the surface of Phobos and Deimos. Looking at general properties of meteorites as possible analogs we notice that while Phobos and Deimos albedos (0.071 ± 0.012, 0.068 ± 0.007, respectively; Britt & Consolmagno 2000) are in the range of darker hydrated meteorites, their bulk density (around 1800 $kg\,m^{-3}$, Witasse et al. 2014) is lower than that of CC meteorites CI, CM (around 2100 $kg\,m^{-3}$) and even lower compared to CO, CR, and CV (around 3100 $kg\,m^{-3}$), in addition no significant evidence of strong hydration appears in the spectra of the moons (Britt & Consolmagno 2000). If the distinct peak in reflectance located near 0.280 μm is confirmed, it likely indicates a significant concentration of sub-microscopic amorphous carbon on the surface of the satellites (Applin et al. 2018). Amorphous carbon on the surface can be caused by an influx of IDPs with a good agreement for albedo and spectral slope (Fries et al. 2017). Differences in slope between blue and red units on Phobos can possibly be explained by different degrees of space weathering on material excavated due to the large impact event that formed Stickney crater. This hypothesis is strengthened by the absence of a relatively large impact crater on Deimos where only red spectra are observed. Following this assumption, highly space weathered anorthosite (99 *wt* per cent plagioclase and 1 *wt* per cent mafic minerals) was proposed as analogue of Martian moons although the match does not fully reproduced the spectral behaviour and some doubt still remains (Yamamoto, Watanabe & Matsunaga 2018). Recently, several type of Phobos soil simulant (UTPS series) was developed by the University of Tokyo based on the Tagish Lake meteorite composition to attempt to reproduce the Phobos spectral behaviour and thus infer the physical and mineralogical properties of its surface (i.e. particle size distributions, the packing density, and the mechanical properties). Some comparisons were performed between the simulants and CRISM spectra and although some spectral features are similar, a perfect match was not achieved (Miyamoto et al. 2021). Parallel to laboratory work, studies of the origin of Mars' moons have attempted to estimate the elemental abundance and a possible mineralogical composition for Phobos and Deimos using numerical models of giant impact formation hypothesis derived from the collision between Mars and different type of projectiles such as CCs, comets, planetoids, or even Moon-like impactors (Ronnet et al. 2016; Pignatale et al. 2018).

2 NEW LABORATORY ANALYSIS

The search for a spectral analogue for Phobos and Deimos faces criticalities such as the absence of bands in the near-infrared wavelength range that must relate to general compositional information retrieved from thermal infrared observations and the physical constraints

of the two moons (i.e. albedo, density, grain size, and thermal inertia). Model fitting and laboratory mixing must take into account all the information available trying to identify the most suitable candidate to be a spectroscopic analogue of Phobos and Deimos. In this work rather than finding a definitive analogue for the Martian moons we are willing to cover some of the pivotal aspect on the development of a spectroscopic analogue of Phobos and Deimos presenting some preliminary measurements performed in INAF-Osservatorio Astrofisico di Arcetri and the Institut de Planétologie et d'Astrophysique de Grenoble (IPAG).

2.1 Materials and methods

We used Mars soil and CC simulants acquired by Exolith Lab funded by Center for Lunar & Asteroid Surface Science at University of Central Florida (Britt et al. 2019; Cannon et al. 2019). We added to the sample set a mineral mixture ($50/50wt.$ per cent plagioclase bytownite and pyroxene augite) to resemble a basaltic composition, a synthetic amorphous carbon (SAC) produced in laboratory by arc discharge (Bussoletti et al. 1987; Colangeli et al. 1993) and antigorite, one of the common form of serpentine (grain size < 10 μm sieved by sedimentation) from Norway acquired by a private seller (characterized in Fornaro et al. 2018). Moreover, we added to the sample set also two carbonaceous meteorites: WIS91600 (Potin et al. 2020) and Tarda (Marrocchi, Avice & Barrat 2021) suggested to be good analogues for Phobos and Deimos.

The Exolith Lab CCs simulants (sCC) were designed to replicate the mineralogy and physical properties of the corresponding meteorites and anticipated asteroid surface materials as closely as is reasonably possible for bulk amounts, from a spectroscopic point of view there are analogies and differences between the simulants spectra and the corresponding CC samples (Britt et al. 2019).

In the giant impact scenario, a fraction between 35 per cent and 50 per cent of Martian material is expected in the bulk composition of Phobos and Deimos (Hyodo et al. 2017), but also in the case of an asteroid capture the possibility of later exogenic contamination from Mars on Phobos and Deimos surface is possible although with percentage decisively lower, about 1 per cent (Hyodo et al. 2019). Considering all these hypotheses, we decided to prepare four mixtures of sCC with Mars simulant (sMARS) in three different proportions: 10 wt. per cent, 30 wt. per cent, and 50 wt. per cent in order to study some combination in the range of proportion derived by previous work (e.g. Hyodo et al. 2017). We also mixed the SAC with the basaltic mixture in 10 wt. per cent, 30 wt. per cent, and 50 wt. per cent and finally, we mixed the SAC with 1wt. per cent of serpentine. All the pure samples and the mixtures used in this work with the detail on the grain size are reported in Table 1.

The first part of laboratory measurements involving the mixtures of two components were performed at INAF-Astrophysical Observatory of Arcetri in Firenze, Italy. The laboratory is equipped with a Bruker VERTEX 70v interferometer interfaced with Harrick Praying Mantis™ for DRIFTS analysis in biconical off-axis geometry. DRIFTS analysis allows accurate determination of the reflectance profile by measuring diffuse reflectance at azimuthal angle 90° with respect to the principal plane (inc. ang. 45°, emiss. ang. 45° and phase ang. 90°). Two optical configurations were used to measure the spectrum between VIS/NIR and medium infrared (MIR) ranges. To measure the range between 0.5 and 1.25 μm (20 000 and 8000 cm^{-1} in wavenumber), the spectrometer is equipped with a Q4238/7 NIR/VIS tungsten lamp, InGaAs Ge and Si detector, and CaF2 optical components. While using an MIR Globar source, DTGS detector and optical elements in KBr, we can scan a wavelength range between

Table 1. Sample set with description, grain size, and components percentage for mixed samples.

Name Samples	Description
sCI	CI simulant[a] in grain size < 500 μm
sCM	CM simulant[a] in grain size < 500 μm
sC2/TL	C2 (Tagish Lake) simulant[a] in grain size < 500 μm
sCR	CR simulant[a] in grain size < 500 μm
sMARS	Jezero crater simulant[a] in grain size < 500 μm
basaltic mix	50/50 bytownite + augite mix in grain size < 200 μm
SAC	Synthetic amorphous carbon in grain size < 1 μm
antigorite	Phyllosilicate serpentine with grain size < 10 μm
WIS91600	CM-anomalous meteorite powder
Tarda	C2-ungrouped meteorite powder
mixtures	
MIX #01	sCI + sMARS at 50, 30, and 10 wt. per cent
MIX #02	sCM + sMARS at 50, 30, and 10 wt. per cent
MIX #03	sC2/TL + sMARS at 50, 30, and 10 wt. per cent
MIX #04	sCR + sMARS at 50, 30, and 10 wt. per cent
MIX #05	SAC + basaltic mix at 50, 30, and 10 wt. per cent
MIX #06	SAC + antigorite at 1 wt. per cent

[a]Simulants were produced by Exolith Lab funded by the Florida Space Institute and CLASS. For the detailed composition, the reader can refer to the Appendix.

1.25 to 25 μm (8000 and 400 cm^{-1} in wavenumber). Spectral resolution during acquisition was 4 cm^{-1} for the VIS/NIR range and 2 cm^{-1} for the MIR, each final spectrum was the result of the average of five single spectra. Reference material was Spectralon™ and Infragold™ from Labsphere for VIS/NIR and MIR ranges, respectively. The intensity acquired in the two configurations match quite well in general, discrepancies that may appear are corrected by scaling the VIS/NIR range to the level of MIR range since the performances of the instrument in the latter are better as stated by the manufacturer. In the Appendix (see Fig. A1), some examples of spectra on both ranges are provided.

In order to study geometry effects, the reflectance spectra of the Mars simulant and two meteorites (Tarda and WIS 91600) were measured over the wavelength range of 500−4000 nm every 10 or 20 nm (see the Appendix, Table A1 for reference) at atmospheric pressure using SHADOWS experimental apparatus at IPAG (Potin et al. 2018). In this apparatus, the light sources is a 250W quartz–tungsten halogen commercial lamp, while a silicon photodiode detector can cover the range from 185 to 1200 nm and a InSb photovoltaic detector is used for the infrared range. The incidence and emergence angles were set in several combinations: (i) 0° and 30°, (ii) 30° and 0°, (iii) 60° and 30°, and (iv) 30° and 60°. The measured surface area was ∼0.5 mm in diameter. Similarly to Arcetri measurements, the reflectance standards were Spectralon™and Infragold™ from Labsphere.

Some parameters were evaluated for a more detailed analysis on the relation between the spectra and the simulant composition. In detail, spectral slope was evaluated using a linear fitting between 1.25 and 2.5 μm, while the hydrated band depth at 2.7 μm was estimated in continuum removed spectra as the intensity difference between the band limits and the band peak.

2.2 Laboratory results

In Fig. 1, we reported the spectra for the six mixtures prepared with the different wt. percentage. Moreover, each simulant was prepared

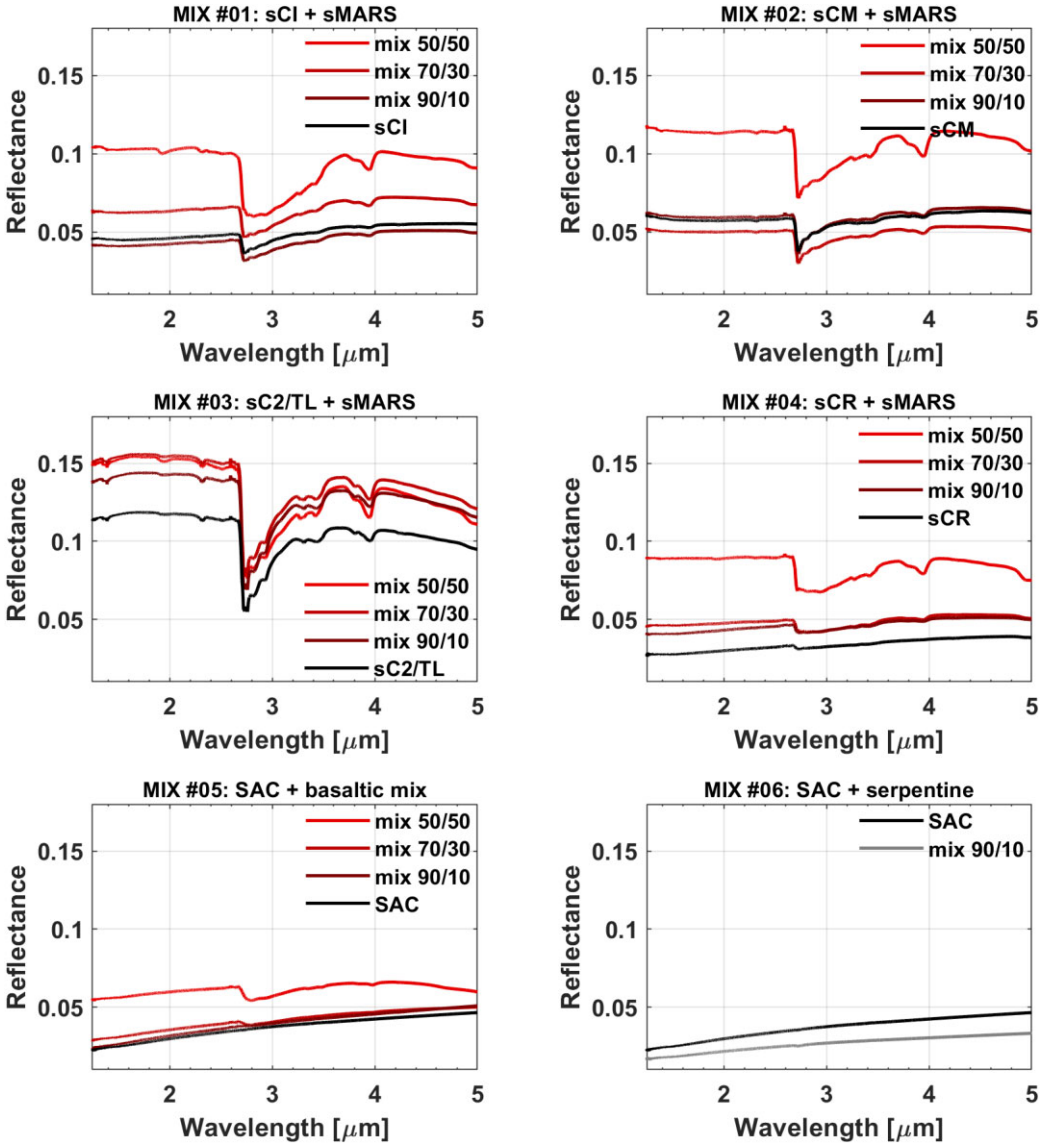

Figure 1. Two component mixtures samples in the NIR range. Mixture from #01 to #04 were produced mixing CCs simulants (sCC) with Mars simulant (sMARS), each combination was mixed with decreasing sMARS component in *wt*.50 per cent, 30 per cent, and 10 per cent with respect to the CC simulant. CCs simulant used are sCI in MIX #01, sCM in MIX #02, sC2/TL in MIX #03, and sCR in MIX #04. For MIX #05, we used SAC with a basaltic mixture (50/50 bytownite & augite) in wt.50 per cent, 30 per cent, and 10 per cent. MIX #06 components are SAC and serpentine in wt.1 per cent. The *Y*-axis range is the same for all the spectra in order to compare differences in absolute reflectance. While the spectra of sCC and SAC are shown along the mixture spectra, the spectrum of Mars simulant was not included in the plot for clarity (the reflectance is more than double with respect to the reflectance of sCC and mixtures) and is shown in the Appendix (Fig. A1).

mixing several minerals in proportions resembling the average composition of the meteorite or Mars class; the exact composition for each simulant sample is listed in the Appendix.

Focusing on MIX from #01 to #04 where Mars simulant was mixed with sCC, we noticed a very neutral, or in some case blue, slope in the NIR range. As well as the original CC meteorites that these samples are simulating and the asteroids that are believed to be their parent bodies (i.e. carbonaceous asteroids), not strong red slopes are observed also in simulated samples. This blue slope is not well matching the observations of the martian moons where both blue and red unit on Phobos and the average of Deimos are characterize by red slopes. The redder spectrum is obtained in the case of MIX #04 using sMARS and sCR, the effect is related to the abundance of pyrite and iron-nickel metal in sCR (not present in the other simulants) and the lowest content of hydrated mineral (serpentine is at 9 per cent while it is between 30 per cent and 70 per cent in the sCM, sCI, and sC2/TL). Iron and iron sulphide are claimed to be the product of space weathering inducing an effect of reddening on the spectral slope (Keller & McKay 1997; Pieters et al. 2000; hapke 2001; Noble, Pieters & Keller 2007; Trang et al. 2021).

Generally, adding a sCC to sMARS we observed a decrease of the absorption band depth and reflectance. Although sCC samples contain a substantial amount of hydrated minerals, the hydrated band at 2.7 μm is considerably reduced up to 96 per cent with respect to the hydrated band of sMARS sample. Hydrated band reduction is not exclusively linked with the relative abundance of hydrated mineral but also with the presence of other components in the total bulk mineralogy: for example both sCM and sCI have a highest abundance

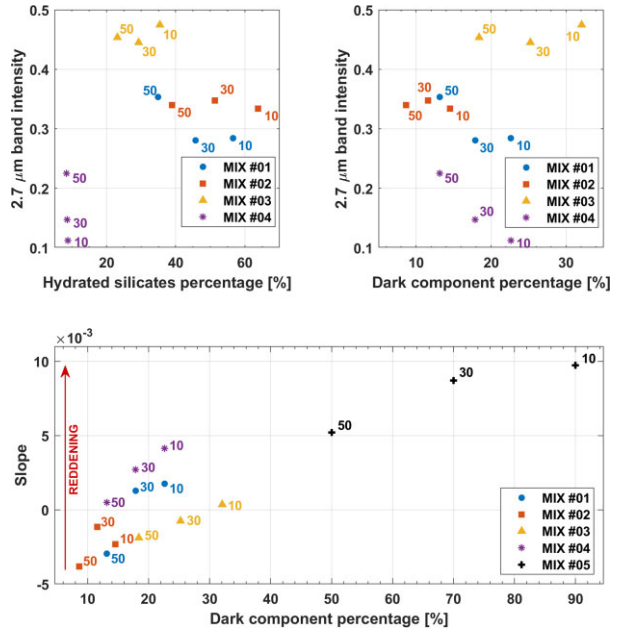

Figure 2. Band parameter for the mixture analysed in our work (in synthesis: MIX #01 sCI+sMARS, MIX #02 sCM+sMARS, MIX #03 sC2/TL+sMARS, and MIX #04 sCR + sMARS; see Table 1 for more detail). Left-hand panel, reflectance evaluated at 1.5 μm and slope evaluated between 1.25 and 2.5 μm. Right-hand panel, reflectance evaluated at 1.5 μm and depth of the hydration band at 2.7 μm. The numbers next to the data point represent the wt. per cent of sMARS component in the mixtures.

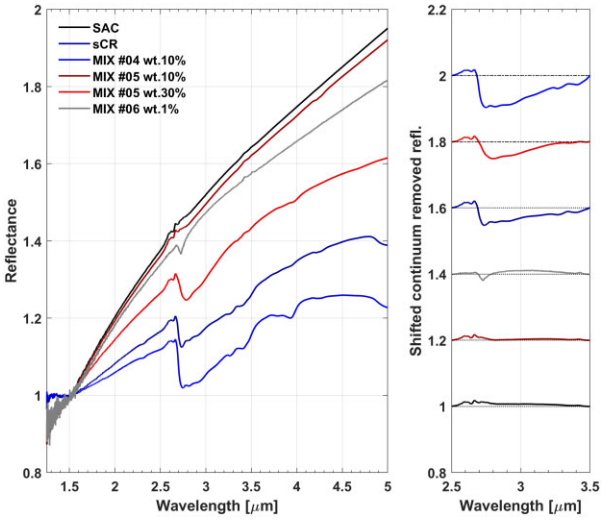

Figure 3. Left-hand panel, best analogue laboratory spectra for matching Phobos and Deimos in the NIR range. In detail: synthetic amorphous carbon (SAC), mixture of sCR with sMARS in 10 wt. per cent (MIX #04), SAC mixed with basaltic mixture, 50/50 bytownite and augite (MIX #05) in 10 wt. per cent, and 30 per cent of the basalt component and SAC mixed with serpentine at 1 wt. per cent. Right-hand panel, details of hydrated band at about 2.7 μm of spectra in left-hand panel after continuum removed and offset for clarity.

of hydrated silicates with respect to sC2/TL but decreasing the abundance of sMARS in the mix the hydrated band is not varying homogeneously in the three samples and is more visible in the mix with sC2/TL (Fig. 1, top panels and central left-hand panel).

In order to increase the goodness of the spectral matching and to preliminary explore other possibilities we produce two additional mixtures using SAC, suggested to be a possible dark component (Fries et al. 2017). The MIX #05 and MIX #06 were obtained mixing SAC respectively with a basaltic mixture, 50/50 plagioclase and pyroxene, and with serpentine in small grain size. As described in the method section, MIX #05 was prepared in the wt. percentage analogue to the previous mixtures while MIX #06 was prepared only at wt.1 per cent of serpentine in order to evaluate the effect of a very small amount of hydrated material. Fig. 1 (bottom panels) shows that SAC used as a dark component is more effective in reducing the spectral intensity and inducing slope reddening than the sCC samples. We noticed also that absolute reflectance in the case of MIX #06 is slightly lower than pure SAC, being the amount of serpentine very small this difference is probably related to instrumental uncertainties due to the very low intensity of the sample.

In order to evaluate the effect of composition on the spectra parameters we studied the possible relation between slope and hydrated band depth at 2.7 μm with abundance of hydrated minerals and dark component (the sum of magnetite, pyrite, iron-nickel, sub-bituminous coal and/or SAC). Results are shown in Fig. 2. MIX #05 was analysed only in the the relation between slope and dark component because officially the composition do not contain hydrated minerals and the presence of a band at 2.7 μm is likely related with OH defects in the matrix of bytwonite and/or augite. MIX #06 was not included being not fully comparable to the rest of the sample set. The Fig. 2, bottom panel, shows the more clear relation: increasing the dark component spectral slope is becoming redder. This is confirmed using all the mixture we have in our sample set with a percentage of dark component varying from 8 per cent to 90 per cent. Looking at the variation of 2.7 μm band depth according to hydrated mineral percentage (Fig. 2, top left-hand panel) we observe an apparent contradiction: increasing the amount of hydrated mineral the band depth linked with this component is generally decreasing. MIX #03 and MIX #04 show different behaviour with, respectively, constant band depth as the percentage changes and decreasing band depth with nearly constant percentages. To interpret this graph we can resort to the upper right-hand panel in Fig. 2, here the relationship between abundance of the dark component (magnetite, pyrite, etc.) and the band depth at 2.7 μm due to hydration is shown. It can be seen that by increasing the dark component, and consequently reducing the intensity, the band depth decreases. The case of MIX #03 is the only one that does not totally follow this trend but it is also the sample with the highest absolute reflectance value in the data set. This result can be interpreted as the fact that the dark component, although in significantly smaller percentages than the hydrated minerals, dominates the appearance of the final spectrum in terms of both slope and band depth.

The study of possible mixtures as analogues of Phobos and Deimos presented here with some preliminary results will need to be further investigated in the years leading up to the arrival of MMX in the Martian system.

Mixtures of basaltic material with SAC and mixture of Mars and sCR (Fig. 3, left-hand panel) represent the best spectroscopic analogues in the NIR range for both Phobos and Deimos. While sCR is made by roughly 34 per cent olivine and pyroxene, 14 per cent magnetite and 9 per cent serpentine (plus other minor components at 5 per cent or less), when mixed with sMARS the anhydrous component of the sample is even higher. All these spectra show a red slope in the range of1–5 μm, reduced hydrated band at 2.7 μm, and almost total absence of minor bands. In detail, sCR and its mix with sMARS show a bluer slope with respect to SAC and its mix with either serpentine or the basaltic mixture. Regarding the depth of

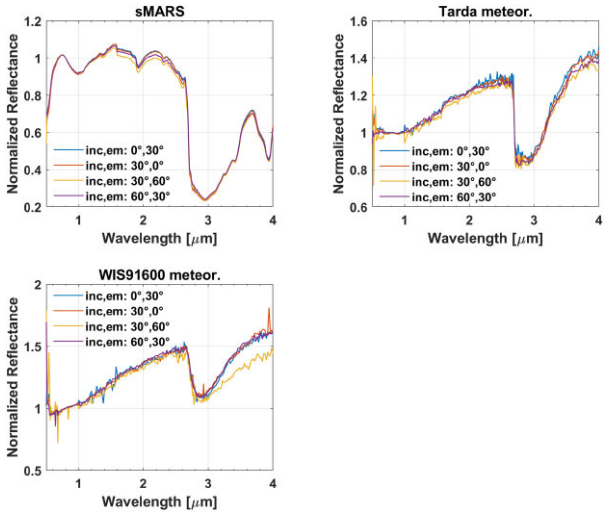

Figure 4. Laboratory spectra in the range 0.5 –4 μm of sMARS, Tarda and WIS 91600 meteorites acquired at IPAG. Four combinations of geometry on incidence angle and emission were measured: (0°, 30°), (30°, 0°), (30°, 60°), and (60°, 30°), all the spectra are normalized at 0.8 μm in order to magnify differences in slope and band depth, original spectra with error bars are shown in the Appendix (Fig. A2). The differences at longer wavelength for WIS91600 spectrum acquired at inc. angle 30° and emiss. angle 60° could be related to the imperfect correction for a grating badly positioned.

the hydrated band, only the sCR and its mixtures along with the mix of SAC and basaltic mixture show a clear feature at 2.7 μm. Mixture of SAC and serpentine in grain size < 10 μm with 10 wt. per cent show a clear feature with a reduced depth compared to the other mixture. Additional analyses on sMARS and the two meteorites of our sample set (Tarda and WIS 91600) were performed, using the IPAG measurement apparatus. Four combinations of geometry on incidence angle and emission were measured: (0°, 30°), (30°, 0°), (30°, 60°), and (60°, 30°), the normalized spectra are shown in Fig. 4 while the original spectra with error bars are shown in the Appendix (Fig. A2). As visible from the original spectra in the Appendix, the variation of incidence and emission angles mainly affects the reflectance, in particular in the range 0.5–2.5 μm, where we observe variations of almost 10 per cent. No strong changes in slope or band depth was observed except for the WIS 91 600 meteorite in geometrical combination (inc. 60°, emis. 30°), where the differences at longer wavelength (> 2.830 μm) could be related to the imperfect correction for a grating badly positioned more likely than a true geometric effect, which is absent in the other samples,

3 COMPARISON WITH REMOTE SENSING DATA

3.1 Comparison in the NIR range

Comparing the laboratory data with observations of Phobos and Deimos in the NIR, it is quite obvious to specify that several combinations may be optimal to match the observations underlying the ambiguity in identifying a single analogue for Phobos and Deimos. This is because the absence of absorption bands and red slope are common to many compounds. The data obtained so far (Fig. 5), and reviewed in detail in the first section of this paper, show good agreement especially considering the large errors associated with some ground-based observations. We chose some lab spectra to compare with the red unit and blue units of Phobos. In this work, Deimos average spectrum was not considered due to its close analogy with Phobos red unit as shown in the left-hand panel of Fig. 5 .

Among the lab spectra, we selected some mixture and the two meteorites with the best agreement with observational data. In the right-hand panel of Fig. 5, the comparison with laboratory data shows a good agreement with Phobos data in term of slope with MIX #05 and #06, SAC based, for the red unit of Phobos (and therefore Deimos average spectrum), while MIX #04 and the proportions of minerals used in the sCR sample are more representative of Phobos blue unit. This does not imply that Phobos is similar to a CR meteorite, but that the combination of minerals used for the simulant are close to a possible combination to reproduce the surface of the moon, even if the sCR itself does not have an optimal match with the real CR meteorites in the available collections (Britt et al. 2019). Tarda and WIS 91 600 meteorites match in terms of slope, respectively, the blue and red units of Phobos, although it is not straightforward to associate the absence of deep hydrated bands to the overall absence of hydrated minerals. The mixes analysed in this work always contain a certain amount of hydrated minerals also if the 2.7 μm band is not really prominent. Therefore, it is challenging to assume that not much hydrated material is present on Phobos and Deimos just because of the absence of a deep band at 2.7 μm.

Regarding the hydrated band comparison is more difficult due to either the lower quality of data of Martian moon observations and the generally deeper band shown by the laboratory spectra. However, we can say that the SAC and sCR mixtures with 10 per cent basaltic mixture and sMARS, respectively, show a comparable trend to the observations, the 1 per cent serpentine mixed with SAC is probably too little for a good match with the Phobos red unit. To understand, however, where are the major difficulties in looking for a spectroscopic analogue of the moons of Mars we must also include the thermal infrared range.

3.2 Comparison in the MIR range

Although only few Phobos observations were performed in the thermal infrared, this wavelength range presents some pivotal spectroscopic features for mineralogical interpretation: CF related to mineralogy and grain size, Reststrahlen bands (RBs) related to mineralogy and Transparency features (TFs) linked with volume scattering of very small grains.

Phobos CF positions retrieved from several TES spectral (Giuranna et al. 2011) classes in and around Stickney crater were associated with average CF position of ultramafic rocks measured in vacuum and, using a more wide range of measurements in air, with single CF positions of nesosilicates, phyllosilicate and partially tectosilicate (Giuranna et al. 2011). Distinguishing red and blue units some differences in CF positions were observed, while the blue unit inside and around Stickney shows a single peak around 8.83 μm, the red unit shows a doublet at 9.59 μm and 9.17 μm (Glotch et al. 2018). In Fig. 6, comparing the CF position of Phobos with data from different classes of meteorites measured in air (Salisbury et al. 1991), the range observed in spectra around Stickney region (grey area in the plot) match with a very large number of meteorite classes although CCs are just partially covered, while HED, Mars meteorite shergottites and E/H/L chondrites are providing a better match. While the Phobos blue unit is falling in between LL and CI/CM groups the two distinguished CFs of the red unit are falling, respectively, in the HED/Shergottite/Ureilite position and the CI/CM/CO group position. Complex CF with doublet can occur when two different major components show their single CF at such distant wavelengths that they do not average in a single peak (Salisbury et al. 1991). Due

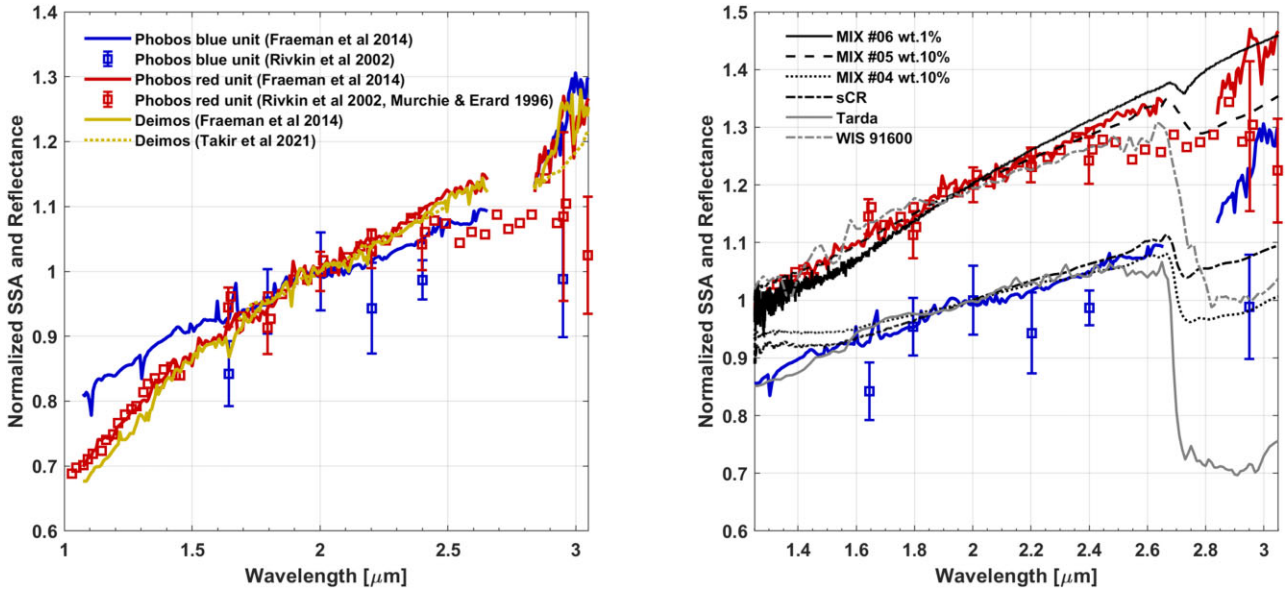

Figure 5. Left-hand panel, selection of ground-based and spacecraft data of Phobos (both red and blue units) and Deimos. All spectra are normalized at 2 μm in order to show differences in slope that characterize the two spectral types observed on the moons. All the spectra show a good agreement considering the large error bars of some ground-based observations. Right-hand panel, comparison between selected spectra of Phobos and laboratory analogues. Spectra of the red unit and blue unit are normalized at 2 μm and offset for clarity. We compared the mixture (black lines) and meteorites (grey lines), showing the best match with the observation. Although the agreement with the slope is pretty good in the studied range, the comparison in the region of the 2.7 μm hydrated band is of lower quality due to both the worse quality of the Phobos spectra and the more intense bands of some laboratory spectra.

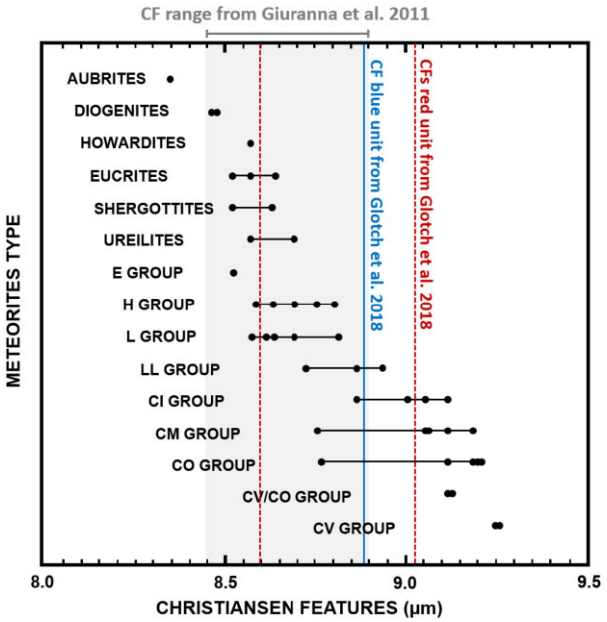

Figure 6. Comparison of observed CF on Phobos with the mean values of CF for different classes of meteorites measured in air (adapted from fig. 9 in Salisbury, D'Aria & Jarosewich 1991). Grey area represents the different range of CFs observed in several TES spectra classes analysed by Giuranna et al. (2011), solid and dashed vertical lines are the values evaluated by Glotch et al. (2018), respectively, for the CF of blue unit and the CF doublet observed in the red unit.

to the large footprint of TES observation on the surface of Phobos (resolution of 2−7 km/pxl at altitude between 275 and 785 km) it is not easy to attribute the CF doublet to different areas with different mineralogy or different components mixed in the same area.

Interestingly, ureilites are well-matching CF position (both with Giuranna et al. 2011 reported range and one of the Glotch et al. 2018 evaluated red unit values). Ureilites are a heterogeneous group of achondrites an nowadays a definite parent body of this meteorite class is still missing although, after the finding of Almahata Sitta meteorite fall in 2008 from asteroid 2008TC3, the F-type asteroids (a less hydrated B-type; Tholen 1984) were proposed as a probable parent body. Having both primitive and differentiated characteristics, ureilite meteorites are possible analog that need to be studied more in detail.

For the MIR range, we compared our mixtures and pure sample spectra to PFS data from Giuranna et al. (2011). the observed spectra are acquired in reflectance and in order to be compared with remote sensing data they were converted in emissivity using the formula $E = 1 - R$. As clearly visible in the Fig. 7, neither pure simulants or mixtures are able to fully match the observations and samples that were good spectroscopic analog in the NIR range are failing to reproduce observations in MIR range. Several pure simulant and mixture (all in the 30 wt. per cent except for MIX #05 at 50 wt. per cent and MIX #06 at 1 wt. per cent) show a deep valley around 11 μm. However, only the basaltic mixture shows the smaller peak at 12 μm that can be observed in PFS data from orbit 5870 and 0756. sCI, and sCM, although with smaller intensity, are the only sample presenting a small peak at 15 μm as well as observation in orbit 5870, but the peak disappear in the mixture at 30 wt. per cent with sMARS (MIX #01 and #02). Amorphous carbon mixture (MIX #05 and #06) with the reduced spectral contrast are not well matching the PFS observations despite being among the best matches in the NIR range. No one of the analysed samples show the broad and intense band at 16.6 μm present in observation of orbit 0756 and 5851 linked by the author to the presence of tectosilicates. In the basaltic mixture, the presence of bytownite (a tectosilicate of the feldspar group) induces a peak around 17 μm but is not well matched with observations. Although there are no planned missions with

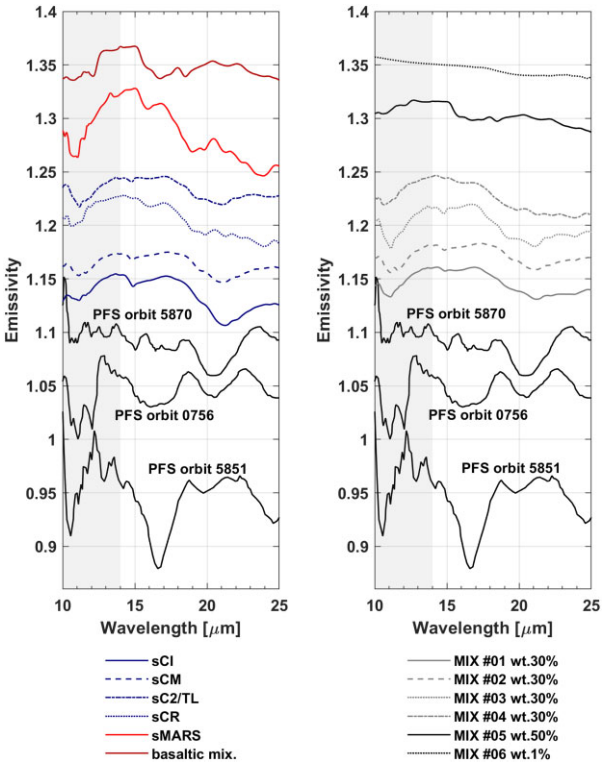

Figure 7. Comparison of PFS remote sensing data of Phobos from Giuranna et al. (2011) and laboratory measurements acquired in INAF-Astrophysical Observatory of Arcetri laboratory in reflectance and converted in emissivity using the formula $E = 1 - R$ to allow qualitative comparison. Bottom solid black lines in both the panels are digitized spectra from Giuranna et al. (2011) (refer to the original publication for spectra errors, grey area highlight the range with the higher noise), each spectra is labelled with the number of the orbit when it was acquired. Blue lines, with different styles, and red lines in the left-hand panel represent the pure simulant component (respectively the CC and martian/basaltic simulants). Grey and black lines, with different styles, in the right-hand panels represent the mixture prepared in the lab. Laboratory data were acquired in reflectance and converted to emissivity using the formula $E = 1 - R$ in order to allow a qualitative analysis.

instruments in the thermal infrared for the observation of Phobos and Deimos, the better resolution and uninterrupted data that will be obtained from MIRS will help to place constraints on the possible interpretations of the data available today.

4 CONCLUSIONS

Phobos and Deimos's composition are still largely unconstrained today. Although several infrared data have been collected by both spacecraft and ground-based observatories, there is still no agreement on the interpretation of these data. These uncertainties reflect the ongoing debate on the origin of Martian moons and their evolution. The MMX mission will aim to shed light on this topic, and the role of the MIRS spectrometer will be pivotal in this regard. MIRS, with its unprecedented spatial resolution, high S/N and a spectrum without interruption (Barucci et al. 2021), will allow us to characterize the composition in detail and to investigate heterogeneity associated with the surface morphology. Numerous hypotheses have been made up today to explain the observed spectroscopic behaviour, although none is definitive. It is still unclear whether the hydrated component observed in the spectra is native to the moons or is a product of *H* implantation through space weathering. A basaltic component appears to dominate the entire surface and probably also the interior thanks to thermal infrared observations of Stickney crater and its ejecta.

Our preliminary laboratory measurements confirm that the red unit of Phobos and most of the surface of Deimos can be associated with samples characterized by an higher presence of dark components (e.g. SAC) or minerals produced by space weathering (e.g. iron-nickel metal and iron sulphide). Presence of dark component could be also totally responsible for the reduced hydrated band observed on the moons without invoking dehydration or implantation on anhydrous surface. On the other hand, the blue unit of Phobos, associated with Stickney crater and its ejecta, could be linked to more pristine material. Phobos red unit appears to be more hydrated, as observed also by previous study, and supported by the association the hypothesis of OH implantation cannot be totally excluded.

This work represents a starting step in the challenge of finding a spectroscopic analogue of Martian moons. Additional measurements will be made within the framework of the MMX mission and the development of the MIRS instrument.

ACKNOWLEDGEMENTS

Simulant samples used in this work were produced by the ExolithLab (Florida Space Institute and The Center for Lunar & Asteroid Surface Science at UCF). They were acquired through the laboratory website or they were shared personally by D. Britt to INAF-Arcetri laboratory. This study was carried out in support of the MIRS instrument financed by CNES.

DATA AVAILABILITY

The data underlying this article will be shared on reasonable request to the corresponding author.

REFERENCES

Applin D. M., Izawa M. R., Cloutis E. A., Gillis-Davis J. J., Pitman K. M., Roush T. L., Hendrix A. R., Lucey P. G., 2018, Icarus, 307, 40
Barucci M. A. et al., 2021, Earth Planets Space, 73, 211
Bertaux J. L., Montmessin F., Gondet B., Bibring J. P., Rebérac A., Baggio L., 2016, in 47th Lunar and Planetary Science Conference, held March 21-25, 2016 at The Woodlands, Texas. LPI Contribution No. 1903. p. 2177
Bibring J. P. et al., 1992, Adv. Space Res., 12, 13
Bibring J. P. et al., 2004, in Wilson A., Chicarro A., eds, ESA Special Publ. Vol. 1240, Mars Express: the Scientific Payload. ESA Publications Division, Noordwijk, Netherlands, p. 37
Britt D. T. et al., 2019, Meteorit. Planet. Sci., 54, 2067
Britt D. T., Consolmagno G. J., 2000, Icarus, 146, 213
Bussoletti E., Colangeli L., Borghesi A., Orofino V., 1987, A&AS, 70, 257
Cannon K. M., Britt D. T., Smith T. M., Fritsche R. F., Batcheldor D., 2019, Icarus, 317, 470
Christensen P. R. et al., 1992, J. Geophys. Res., 97, 7719
Cloutis E. A., Gaffey M. J., Smith D. G. W., Lambert R. S. J., 1990a, Icarus, 84, 315
Cloutis E. A., Gaffey M. J., Smith D. G. W., Lambert R. S. J., 1990b, Icarus, 86, 383
Cloutis E. A., Hardersen P. S., Reddy V., Gaffey M. J., Bailey D. T., Craig M. A., 2009, in 40th Lunar and Planetary Science Conference, (Lunar and Planetary Science XL), held March 23-27, 2009 in The Woodlands, Texas. p. 1332
Colangeli L., Mennella V., Blanco A., Fonti S., Bussoletti E., Gumlich H. E., Mertins H. C., Jung C., 1993, ApJ, 418, 435
Formisano V. et al., 2005, Planet. Space Sci., 53, 963

Fornaro T., Boosman A., Brucato J. R., ten Kate I. L., Siljeström S., Poggiali G., Steele A., Hazen R. M., 2018, Icarus, 313, 38
Fraeman A. A. et al., 2012, J. Geophys. Res. (Planets), 117, E00J15
Fraeman A. A., Murchie S. L., Arvidson R. E., Clark R. N., Morris R. V., Rivkin A. S., Vilas F., 2014, Icarus, 229, 196
Fries M., Cintala M., Steele A., Welzenbach L. C., 2017, in 48th Lunar and Planetary Science Conference, held 20-24 March 2017, at The Woodlands, Texas. LPI Contribution No. 1964. p. 2570
Gendrin A., Langevin Y., Erard S., 2005, J. Geophys. Res. (Planets), 110, E04014
Giuranna M., Roush T. L., Duxbury T., Hogan R. C., Carli C., Geminale A., Formisano V., 2011, Planet. Space Sci., 59, 1308
Glotch T. D., Edwards C. S., Yesiltas M., Shirley K. A., McDougall D. S., Kling A. M., Bandfield J. L., Herd C. D. K., 2018, J. Geophys. Res. (Planets), 123, 2467
Grundy W. M., Fink U., 1992, in Harris A. W., Bowell E., eds, Asteroids, Comets, Meteors 1991. Lunar and Planetary Society, 3600 Bay Area Boulevard, Houston, TX 77058, p. 215
hapke B., 2001, J. Geophys. Res., 106, 10039
Hartmann W. K., 1990, Icarus, 87, 236
Hesselbrock A. J., Minton D. A., 2017, Nature Geosci., 10, 266
Higuchi A., Ida S., 2017, AJ, 153, 155
Hyodo R., Genda H., Charnoz S., Pignatale F. C. F., Rosenblatt P., 2018, ApJ, 860, 150
Hyodo R., Genda H., Charnoz S., Rosenblatt P., 2017, ApJ, 845, 125
Hyodo R., Kurosawa K., Genda H., Usui T., Fujita K., 2019, Sci. Rep., 9, 19833
Ivanov A. V., 2004, Solar Syst. Res., 38, 97
Keller L. P., McKay D. S., 1997, Geochim. Cosmochim. Acta, 61, 2331
Ksanfomality L. V. et al., 1989, Nature, 61, 2331
Ksanfomality L. V. et al., 1991, Planet. Space Sci., 39, 311
Kuramoto K. et al., 2022, Earth Planets Space, 74, 12
Lucey P. G., Bell J. F., Piscitelli J. R., 1989, in Lunar and Planetary Science Conference. p. 598
Lunine J. I., Neugebauer G., Jakosky B. M., 1982, J. Geophys. Res., 87, 10297
Lynch D. K. et al., 2007, AJ, 134, 1459
Marrocchi Y., Avice G., Barrat J.-A., 2021, ApJ, 913, L9
McCord T. B. et al., 2012, Nature, 491, 83
Miyamoto H. et al., 2021, Earth Planets Space, 73, 214
Murchie S. et al., 2007, J. Geophys. Res. (Planets), 112, E05S03
Murchie S. L. et al., 1991, J. Geophys. Res., 96, 5925
Murchie S. L. et al., 2008, in 39th Lunar and Planetary Science Conference, (Lunar and Planetary Science XXXIX), held March 10-14, 2008 in League City, Texas. LPI Contribution No. 1391. p. 1434
Murchie S., 1999, J. Geophys. Res., 104, 9069
Murchie S., Erard S., 1996, Icarus, 123, 63
Nakauchi Y. et al., 2021, Icarus, 355, 114140
Noble S. K., Pieters C. M., Keller L. P., 2007, Icarus, 192, 629
Pajola M. et al., 2012, MNRAS, 427, 3230
Pajola M. et al., 2013, ApJ, 777, 127
Pajola M., Roush T., Dalle Ore C., Marzo G. A., Simioni E., 2018, Planet. Space Sci., 154, 63
Pang K. D., Rhoads J. W., Lane A. L., Ajello J. M., 1980, Nature, 283, 277
Pieters C. M. et al., 2000, Meteorit. Planet. Sci., 35, 1101
Pignatale F. C., Charnoz S., Rosenblatt P., Hyodo R., Nakamura T., Genda H., 2018, ApJ, 853, 118
Potin S., Beck P., Usui F., Bonal L., Vernazza P., Schmitt B., 2020, Icarus, 348, 113826
Potin S., Brissaud O., Beck P., Schmitt B., Magnard Y., Correia J.-J., Rabou P., Jocou L., 2018, Applied Optics, 57, 8279
Rivkin A. S., Brown R. H., Trilling D. E., Bell J. F., Plassmann J. H., 2002, Icarus, 156, 64
Ronnet T., Vernazza P., Mousis O., Brugger B., Beck P., Devouard B., Witasse O., Cipriani F., 2016, ApJ, 828, 109
Rosenblatt P., Charnoz S., Dunseath K. M., Terao-Dunseath M., Trinh A., Hyodo R., Genda H., Toupin S., 2016, Nature Geosci., 9, 581
Roush T. L., Hogan R. C., 2000, in 31st Annual Lunar and Planetary Science Conference, March 13-17, 2000, Houston, Texas, LPI Contribution no. 1598
Roush T. L., Hogan R. C., 2001, in 32nd Annual Lunar and Planetary Science Conference, March 12-16, 2001, Houston, Texas, LPI Contribution no. 1915
Salisbury J. W., D'Aria D. M., Jarosewich E., 1991, Icarus, 92, 280
Smith N. M., Edwards C. S., Mommert M., Trilling D. E., Glotch T. D., 2018, in 49th Lunar and Planetary Science Conference 19-23 March, 2018, held at The Woodlands, Texas LPI Contribution No. 2083. p. 2809
Takir D., Matsuoka M., Waiters A., Kaluna H., Usui T., 2022, Icarus, 371, 114691
Tholen D. J., 1984, PhD. Thesis, University of Arizona, Tucson, p. 2201
Thomas N., Britt D. T., Herkenhoff K. E., Murchie S. L., Semenov B., Keller H. U., Smith P. H., 1999, J. Geophys. Res., 104, 9055
Thomas N., Stelter R., Ivanov A., Bridges N. T., Herkenhoff K. E., McEwen A. S., 2011, Planet. Space Sci., 59, 1281
Trang D. et al., 2021, Planet. Sci. J., 2, 68
Wiegert P., Galiazzo M. A., 2017, Planet. Space Sci., 142, 48
Witasse O. et al., 2014, Planet. Space Sci., 102, 18
Yamamoto S., Watanabe S., Matsunaga T., 2018, Geophys. Res. Lett., 45, 1305

APPENDIX: SIMULANTS COMPOSITION AND ADDITIONAL INFORMATION

All the simulant samples used in this work were received or purchased by Exolith Lab (Orlando, Florida, USA). Exolith Lab is an at-cost organization largely funded by the Florida Space Institute and CLASS, The Center for Lunar & Asteroid Surface Science at UCF. Exolith Lab develops and produces Lunar, Martian, and asteroid regolith simulants also performing scientific research led by Dr. Dan Britt and Dr. Zoe Landsman. Below the complete fact sheet for the sample used.

Simulant name: JEZ-1 Jezero Delta Simulant (Mars)
Mean and median particle size: 70 μm and 60 μm
Particle size range: $< 0.04 - 500\,\mu$m
Mineralogy (as mixed): Olivine 32.0 wt. per cent, anorthosite 16.0 wt. per cent, glass-rich basalt 13.5 wt. per cent, pyroxene 12.0 wt. per cent, Mg-carbonate 11.0 wt. per cent, Smectite 6.0 wt. per cent, Mg-sulfate 2.4 wt. per cent, ferrihydrite 2.1 wt. per cent, hydrated silica 1.8 wt. per cent, magnetite 1.1 wt. per cent, anhydrite 1.0 wt. per cent, Fe-carbonate 0.8 wt. per cent, hematite 0.3 wt. per cent
Simulant name: CI simulant
Mean and median particle size: 70 and 60 μm
Particle size range: < 0.04–500 μm

Table A1. Acquisition steps in SHADOWS (IPAG, Grenoble) for samples measured in this work. Note the main difference around 2000−2500 *nm*.

WIS91600		
Start (nm)	*End (nm)*	*Step (nm)*
500	1000	10
1020	2500	20
2510	3000	10
3020	4000	20
WIS91600		
Start (nm)	*End (nm)*	*Step (nm)*
500	1000	10
1020	2000	20
2010	3000	10
3020	4000	20

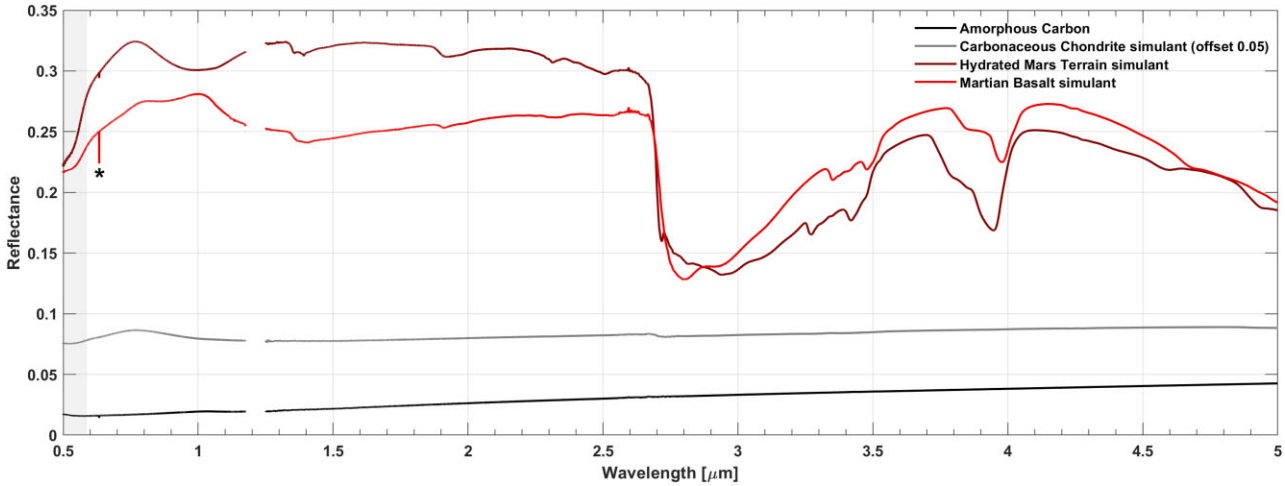

Figure A1. Main components of mixed samples on the full VIS/NIR range of Astrobiology Laboratory at INAF-Astrophysical Observatory of Arcetri. Grey box on the left marks the range where the detector sensitivity is approxing the minimum and therefore the spectrum reliability is lower. Spike feature marked with (∗) is an artefact due to the pointing laser of the spectrometer. Spectra are cutted at 10 μm and not shown up to the limit of acquisition of 25 μm for clarity.

Mineralogy (as mixed): Serpentine 48.0 wt. per cent, magnetite 13.5 wt. per cent, vermiculite 9.0 wt. per cent, olivine 7.0 wt. per cent, pyrite 6.5 wt. per cent, epsomite 6.0 wt. per cent, attapulgite 5.0 wt. per cent, sub-bituminous coal 5.0 wt. per cent

Simulant name: CM simulant

Mean and median particle size: 70 and 60 μm

Particle size range: < 0.04–500 μm

Mineralogy (as mixed): Serpentine 70.0 wt. per cent, magnetite 10.0 wt. per cent, olivine 7.5 wt. per cent, sub-bituminous coal 3.5 wt. per cent, pyrite 2.5 wt. per cent, Pyroxene 2.5 wt. per cent, Sodium metasilicate 3.5 wt. per cent, Siderite 1.0 wt. per cent

Simulant Name: C2 Tagish lake simulant

Mean and median particle size: 70 and 60 μm

Particle size range: < 0.04–500 μm

Mineralogy (as mixed): Serpentine 30.5 wt. per cent, olivine 25.0 wt. per cent, magnetite 22.0 wt. per cent, pyrite 8.5 wt. per cent, sub-bituminous coal 5.0 wt. per cent, vermiculite 4.0 wt. per cent, attapulgite 4.0 wt. per cent, dolomite 1.0 wt. per cent

Simulant name: CR simulant

Mean and median particle size: 70 and 60 μm

Particle size range: < 0.04–500 μm

Mineralogy (as mixed): Olivine 33.0 wt. per cent, pyroxene 31.0 wt. per cent, magnetite 14.0 wt. per cent, serpentine 9.0 wt. per cent, iron–nickel metal 5.0 wt. per cent, pyrite 4.0 wt. per cent, sub-bituminous coal 2.0 wt. per cent, sodium metasilicate 2.0 wt. per cent

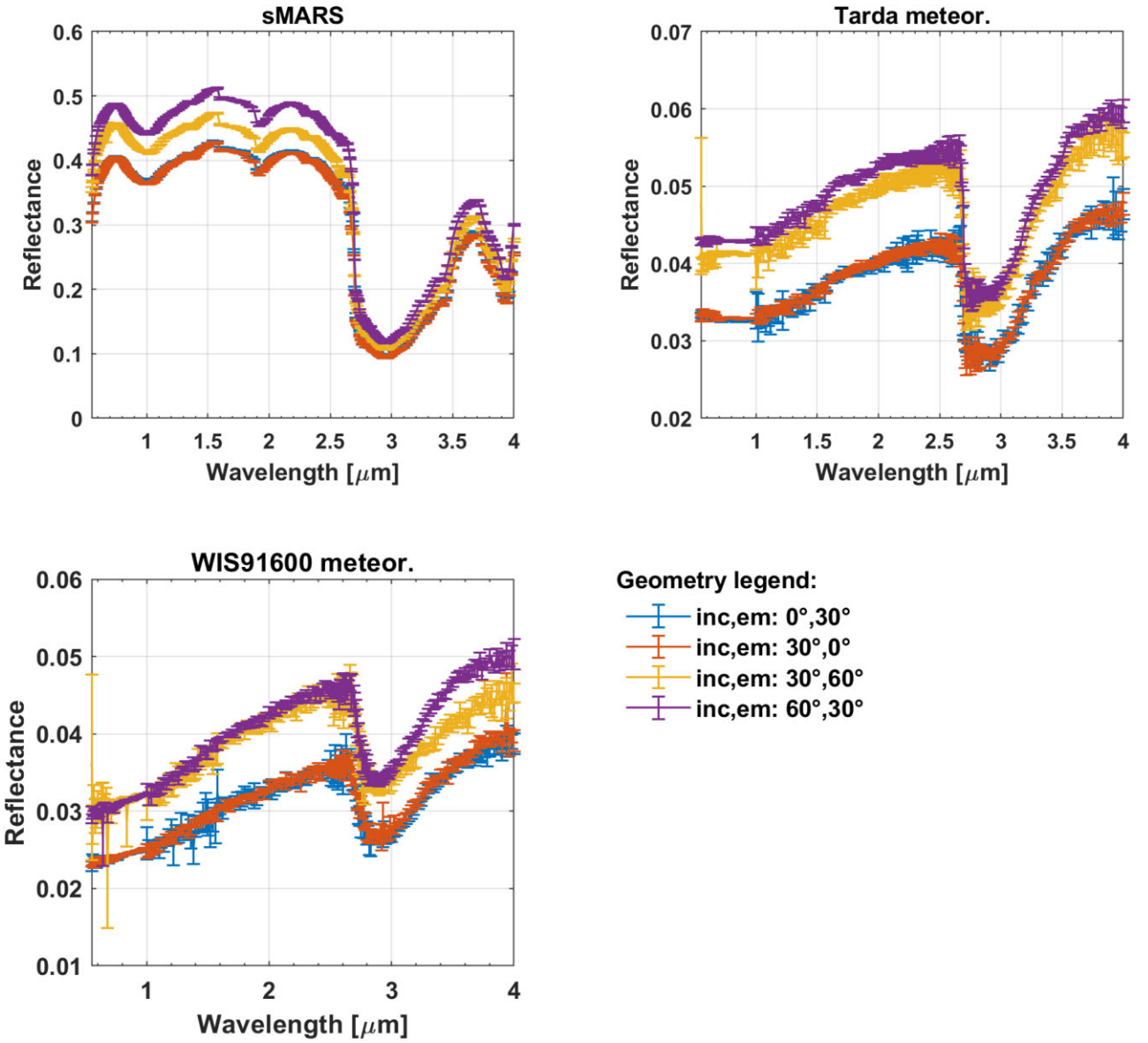

Figure A2. Spectra of Martian simulant, Tarda meteorite and WIS 91600 meteorite with errorbar measured at IPAG laboratory on the full range of acquisition at different geometric configurations for incidence and emission angles. In detail the colour code (same for every panel): blue line for incidence 0° and emission 30°; red line for incidence 30° and emission 0°; yellow line for 60° and emission 30°; and purple for incidence 30° and emission 60°.

This paper has been typeset from a TEX/LATEX file prepared by the author.